JBC RESEARCH ARTICLE

Arginine-rich C9ORF72 ALS proteins stall ribosomes in a manner distinct from a canonical ribosome-associated quality control substrate

Received for publication, May 9, 2022, and in revised form, November 23, 2022 Published, Papers in Press, December 5, 2022,
https://doi.org/10.1016/j.jbc.2022.102774

Viacheslav Kriachkov[1], Angelique R. Ormsby[1], Eric P. Kusnadi[2,3], Hamish E. G. McWilliam[1,4], Justine D. Mintern[1], Shanika L. Amarasinghe[5], Matthew E. Ritchie[5], Luc Furic[2,3,6], and Danny M. Hatters[1,*]

From the [1]Department of Biochemistry and Pharmacology and Bio21 Molecular Science and Biotechnology Institute, The University of Melbourne, Melbourne, Victoria, Australia; [2]Translational Prostate Cancer Research Laboratory, Peter MacCallum Cancer Centre, Melbourne, Victoria, Australia; [3]Sir Peter MacCallum Department of Oncology, University of Melbourne, Parkville, Victoria, Australia; [4]Department of Microbiology and Immunology, Peter Doherty Institute of Infection and Immunity, The University of Melbourne, Melbourne, Victoria, Australia; [5]Walter and Eliza Hall Institute of Medical Research, Melbourne, Victoria, Australia; [6]Department of Anatomy and Developmental Biology, Monash Biomedicine Discovery Institute Cancer Program, Monash University, Clayton, Victoria, Australia

Edited by Karen Fleming

Hexanucleotide expansion mutations in *C9ORF72* are a frequent cause of amyotrophic lateral sclerosis. We previously reported that long arginine-rich dipeptide repeats (DPRs), mimicking abnormal proteins expressed from the hexanucleotide expansion, caused translation stalling when expressed in cell culture models. Whether this stalling provides a mechanism of pathogenicity remains to be determined. Here, we explored the molecular features of DPR-induced stalling and examined whether known mechanisms such as ribosome quality control (RQC) regulate translation elongation on sequences that encode arginine-rich DPRs. We demonstrate that arginine-rich DPRs lead to stalling in a length-dependent manner, with lengths longer than 40 repeats invoking severe translation arrest. Mutational screening of 40×Gly-Xxx DPRs shows that stalling is most pronounced when Xxx is a charged amino acid (Arg, Lys, Glu, or Asp). Through a genome-wide knockout screen, we find that genes regulating stalling on polyadenosine mRNA coding for poly-Lys, a canonical RQC substrate, act differently in the case of arginine-rich DPRs. Indeed, these findings point to a limited scope for natural regulatory responses to resolve the arginine-rich DPR stalls, even though the stalls may be sensed, as evidenced by an upregulation of RQC gene expression. These findings therefore implicate arginine-rich DPR-mediated stalled ribosomes as a source of stress and toxicity and may be a crucial component in pathomechanisms.

GGGGCC hexanucleotide repeat expansion mutations in intron 1 of *C9ORF72* are the most common genetic cause of amyotrophic lateral sclerosis (ALS) and frontotemporal dementia (1, 2). Normally, there are less than 24 repeats, whereas the length is expanded to often hundreds in ALS-causing alleles (3). The expanded GGGGCC leads to the production of sense and antisense mRNA products that display two unusual features that have been postulated to contribute to disease. One is that the mRNA can form granular intracellular foci that contribute to toxicity through RNA-based mechanisms (4). The other is that both sense and antisense mRNA can be translated through alternative initiation codons (*i.e.*, non-AUG translation) to produce five distinct dipeptide-containing polymers (poly-GA, GR, GP, PR, and PA) (5). These abnormal proteins accumulate in the brain of patients with *C9ORF72* mutations. The two arginine-containing dipeptide repeats (DPR), poly-GR and poly-PR, have been shown to be particularly toxic when added to cells or when expressed in cellular and organismal models (6–8). The toxicity is preserved if the GR and PR are encoded by mixed codons, suggesting that the protein sequence itself is directly toxic and therefore not entirely arising from the mRNA (7, 8).

The fidelity of protein synthesis involves mechanisms that detect and eliminate spontaneous cases of aberrant translation (9). This includes translation of mRNAs with various defects: mRNAs with stable stem-loop structures, damaged bases, or other obstacles to elongation (no-go decay), mRNAs that lack stop codons (nonstop decay), and mRNAs with premature stop codons (nonsense-mediated mRNA decay) (10). A marked decrease in elongation rates on such mRNAs can lead to formation of persistent ribosomal collisions, which are targeted for ribosome quality control (RQC) pathway that resolves such stalls and causes degradation of both defective mRNA and polypeptide (11–14). In the event stalls happen aberrantly and remain unresolved, they can have pathological consequences. It was reported that simultaneous mutation of a central nervous system–specific tRNA gene that leads to stalling on specific codons, and the mutational loss of GTPBP2, a ribosome rescue factor resolving such stalls, causes widespread neurodegeneration in mice (15). Similarly, mice with a loss of function of LTN1 protein that targets stalled nascent chains for degradation also exhibited a neurodegenerative phenotype (16).

* For correspondence: Danny M. Hatters, dhatters@unimelb.edu.au.

Recent studies from us and others showed that expression of long repeats of poly-GR and poly-PR causes severe ribosomal stalling (17, 18) and it was proposed that the positively charged R-rich nascent polypeptide electrostatically jams the ribosome exit tunnel (19). However, the mechanisms by which stalling occurs and whether it contributes to toxicity remain unclear. Another outstanding question is whether known mechanisms that target stalled ribosomes in cells are capable of sensing and regulating the aberrant translation of poly-GR and poly-PR proteins. Here, we examined the molecular features of stalling of poly-GR and poly-PR. We examined the length of the repeat required to stall, the specificity of arginine in a context of DPR-mediated stalling, and conducted a screen for potential genetic regulators of stalling on poly-PR protein. Collectively, our findings indicated that the mechanisms involved in stalling caused by long R-rich DPRs appear distinct to the mechanisms leading to stalling on poly-K coded by polyadenosine sequence that mimics defective mRNAs lacking stop codons. Our findings point to a mechanism of toxicity that arises from a poor natural capacity to resolve stalls involving R-rich DPRs, at least in the cell line of our study, and thus, the stalls contribute to an unresolvable state of stress.

Results

Arginine-rich DPRs stall during translation in a length-dependent manner

To find the DPR length at which the nascent chain is long enough to stall translation, we used a series of DNA sequences coding PR and GR DPRs of various lengths: 10×, 20×, 30×, 40×, 50×, 75×, and 102×, where the number indicates the number of DPRs. All DPR-coding sequences were codon-optimized to minimize repetitive mRNA sequences and codon repetitiveness. The efficiency of stalling was assessed using the previously described dual-reporter transcript (Fig. 1*A*) (20–23). Briefly, this reporter consists of a test sequence which is flanked, in frame and without stop codons, with sequences encoding green fluorescent protein (GFP) and mCherry fluorescent protein (ChFP). P2A sequences separate the test sequence from the GFP and ChFP and cause the ribosome to "skip" the glycyl–prolyl peptide bond formation. As such, a single mRNA transcript can translate three separate proteins (24). The ChFP to GFP ratio serves as a measure of whether the test sequence causes stalling, *i.e.*, the ChFP/GFP value will decrease in the event stalling occurs. HEK293T cells were transfected with the dual-reporters, and fluorescence intensities of ChFP and GFP were measured by fluorescence-

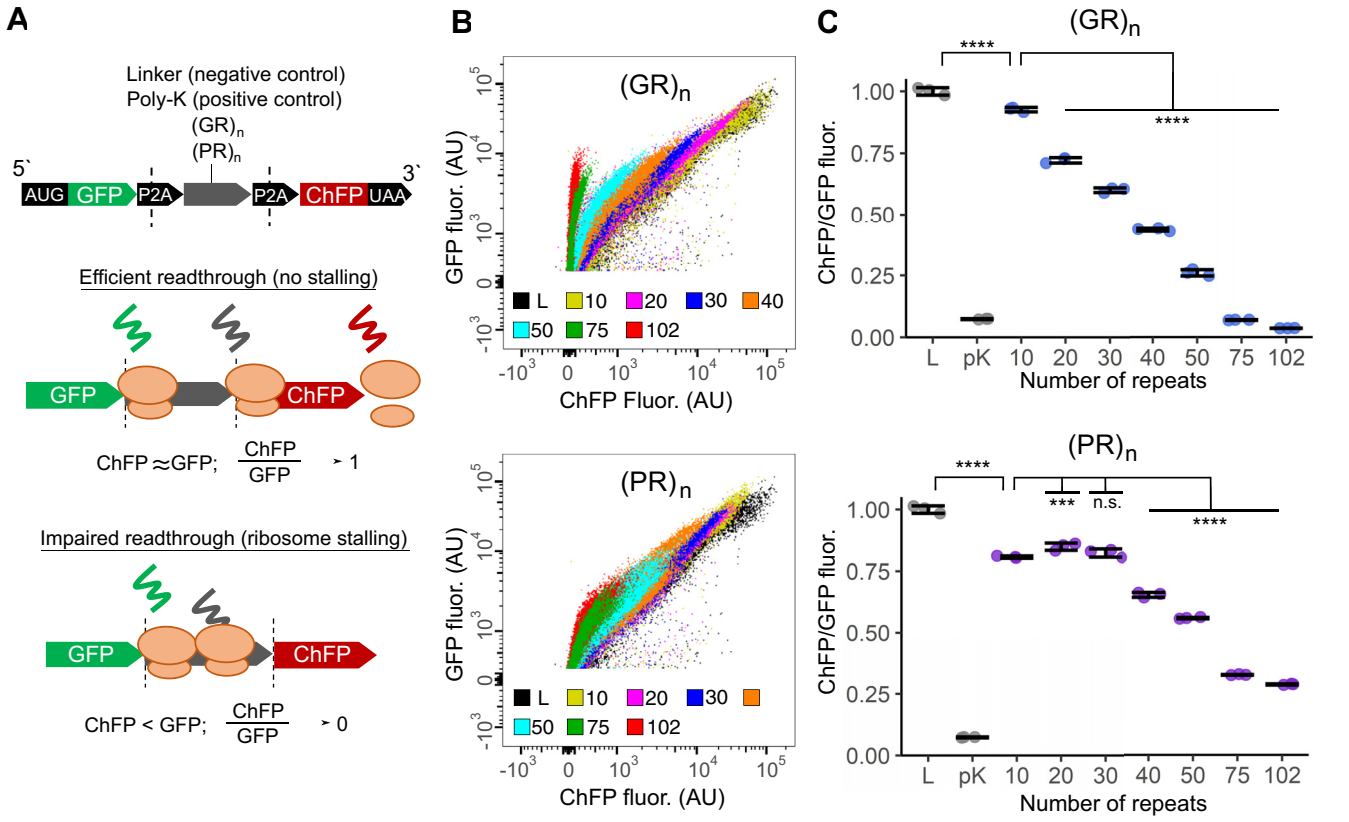

Figure 1. Ribosome stalling assays with poly-GR and poly-PR of different lengths. *A*, schematic of the sequence of the dual-fluorescent stall reporter. *B*, flow cytograms of HEK293T cells 24 h after transfection with poly-GR and poly-PR coding sequences of indicated length (10×, 20×, 30×, 40×, 50×, 75× or 102×) inserted into fluorescent reporter, L – linker. *C*, ChFP/GFP ratios for different poly-PR and poly-GR stall reporters. L – linker, pK – poly-K coded by (AAA) codons. Median GFP and ChFP fluorescence intensity values were measured by FACS, and the resultant ChFP/GFP ratios were normalized to ChFP/GFP ratio of linker control reporter (set as 1). Data represent means, bars show SD, n = 3. Constructs of different lengths and linker control were compared to the shortest DPR (10 repeats) using one-way ANOVA and Dunnett's post hoc test. n.s. – not significant; ***$p < 0.001$, ****$p < 0.0001$. ChFP, mcherry fluorescent protein; DPR, dipeptide repeat; GFP, green fluorescent protein.

activated single cell sorting (FACS). While both poly-PR and poly-GR proteins lowered the ChFP/GFP ratio progressively in a length-dependent manner suggesting increased levels of stalled translation, poly-GR showed higher levels of stalling compared to poly-PR at the same repeat lengths (Fig. 1, *B* and *C*). Based on GFP fluorescence intensities, both DPRs showed decreases in expression levels starting from 20 repeats, which may indicate concentration-dependent toxicity or higher rates of mRNA degradation, and we cannot discount these effects influencing the ChFP/GFP ratios. It is established that Arg is toxic in this format even at 10 repeat lengths but seems more toxic at longer lengths (17) (Additional File 4: Fig. S1). GR appeared to almost completely stall at 75 repeats, whereas PR had a more moderate effect over the range of repeat lengths of study (102 repeats). These findings therefore point to GR being a more effective stalling sequence than PR at comparable repeat lengths.

Charged amino acids in the context of DPR appear to induce ribosome stalling

Given that other nonarginine DPRs associated with *C9ORF72* hexanucleotide expansion (poly-PA and poly-GA) do not appear to lead to stalling (17), we next examined whether stalling in a DPR context was specific to arginine. A panel of DPRs was assessed in the stalling assay whereby each variant was a DPR containing one of 19 amino acids alternating with glycine (Fig. 2*A*). The sequences were codon optimized to minimize secondary structures and codon usage bias where possible. The levels of GFP expression varied between constructs (Fig 2, *B* and Additional File 4: Fig. S2) which may be due to differences in transfection efficiency, mRNA degradation, or DPR-induced cytotoxicity. The DPRs containing charged residues at neutral pH (Arg, Asp, Glu, and Lys) or Trp led to the largest decreases in ChFP/GFP ratios, suggestive of substantial ribosome stalling (Fig. 2, *A* and *D*). Assigning DPRs into three different groups according to their amino acid properties (nonpolar, polar, highly charged) showed that the elongation of highly charged DPRs occurs with significantly lower efficiency compared to DPRs from other groups (Fig. 2*C*). Of these, the negatively charged DPRs (40×GD and 40×GE) appeared more severe in their effect than the positively charged DPRs (40×GR and 40×GK). Prior work has suggested that positively charged amino acid patterning can influence the stalling of translation during synthesis (25). The reduced level of Cherry relative to GFP was confirmed by Western Blot for the reporters containing charged amino acids (Additional File 4: Fig. S3).

Poly-PR translation leads to significant changes in the expression of various stress response genes including the upregulation of RQC genes

To determine whether polyadenosine-mediated stalling induces a similar change in gene expression as the Arg-rich DPR, we performed transcriptome analysis. We focused on the 102×PR construct for the next set of experiments, in part because it has less stalling than the 102×GR and offered a

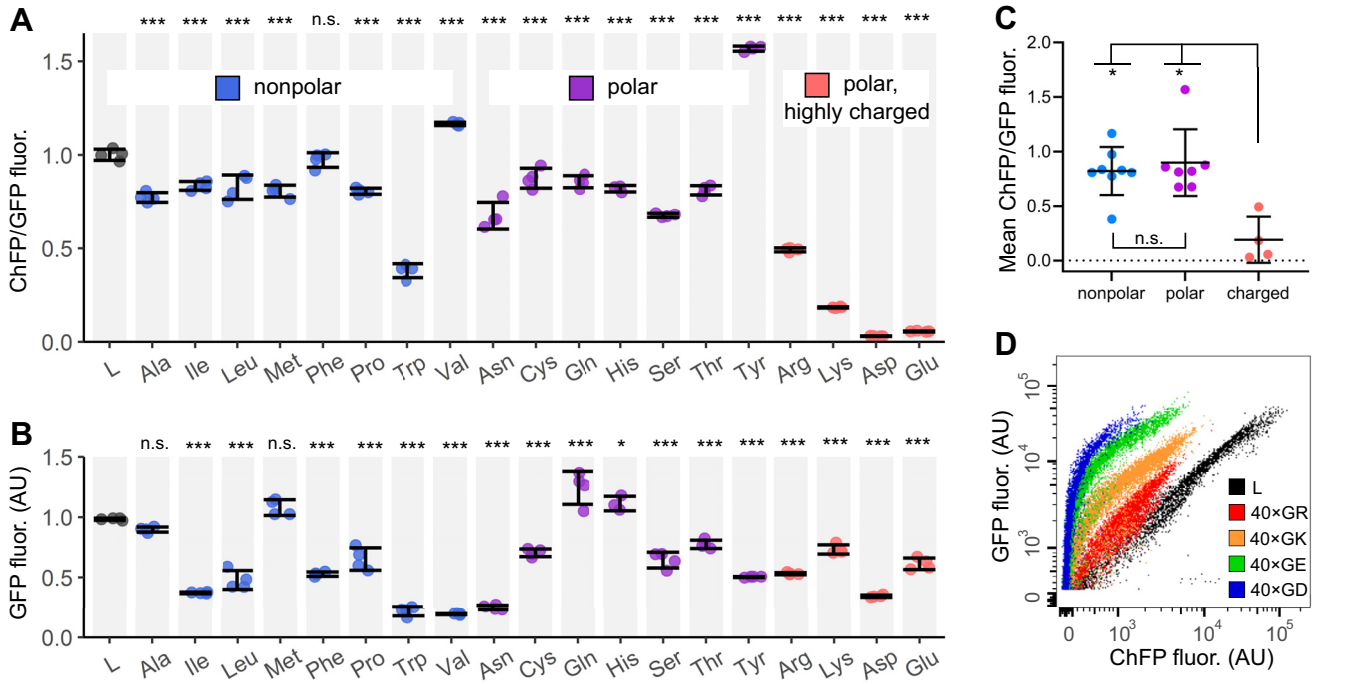

Figure 2. Impact of each amino acid (paired with Gly) on ribosome stalling in a 40 repeat DPR context. *A*, ChFP/GFP ratios and *B*, GFP fluorescence intensities in cells expressing different DPRs were normalized to cells expressing linker control (set as 1). Each DPR is 40×Gly-Xxx, where Xxx—amino acid residue displayed on the x axes. Bars show means and SD of four replicates (*circles*). n.s. – not significant; $^{*}p < 0.05$, $^{***}p < 0.001$ as determined by one-way ANOVA and Dunnett's post hoc test (all values are compared to linker control). *C*, mean ChFP/GFP values of DPRs grouped into three different categories based on DPR amino acid property. n.s. – not significant; $^{*}p < 0.05$ as determined by Kruskal–Wallis rank-based nonparametric test. *D*, flow chart showing ChFP readout of all fluorescent reporters containing charged DPRs: 40×Gly-Arg (40×GR), 40×Gly-Lys (40×GK), 40×Gly-Glu (40×GE), 40×Gly-Asp (40×GE). ChFP, mcherry fluorescent protein; DPR, dipeptide repeat; GFP, green fluorescent protein; L, linker.

greater dynamic range to explore parameters that enhanced or suppressed stalling. We created three stable HEK293T cell lines expressing GFP-P2A-ChFP (which provides a negative control with no stalling), GFP-P2A-poly-K, whereby poly-K was coded with 21 consecutive (AAA) codons (and therefore represents a validated RQC substrate, which induces stalling), and GFP-P2A-102×PR under a Tet-inducible promoter (Fig. 3*A*). Gene expression levels were compared for the poly-K or 102×PR staller *versus* the ChFP negative control. Principle component analysis indicated that 102×PR-expressing cells

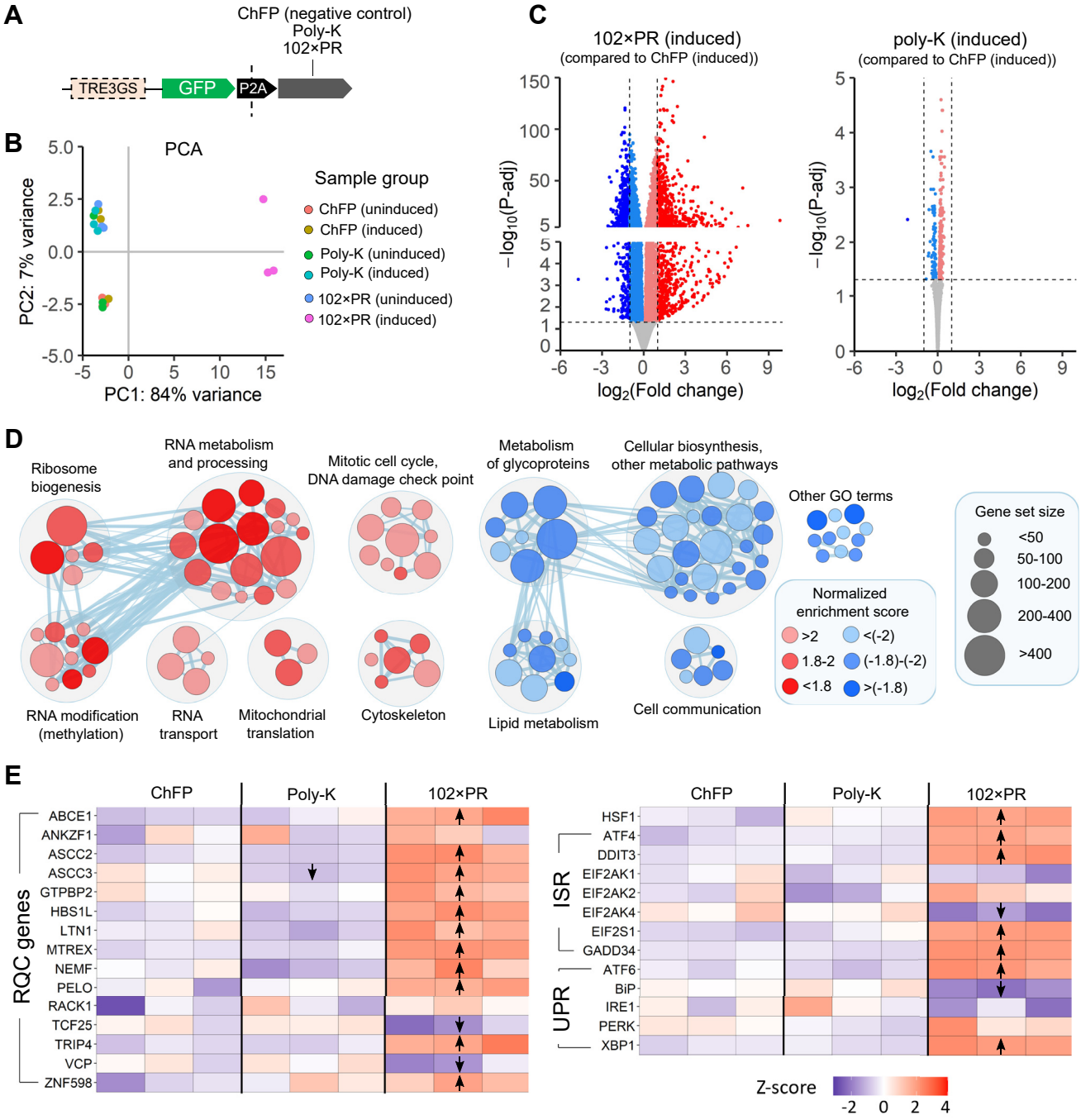

Figure 3. Changes in global transcriptome caused by expression of poly-K or poly-PR stallers. *A*, schematic of the transcript used to generate stable cell *lines*. TRE3GS—promoter containing tetracycline response element (TRE). *B*, principal component analysis plot for all samples. Each group was done in triplicate (n = 3). *C*, volcano plots showing differentially expressed genes (p-adj < 0.05, *horizontal line*) for each staller. *Red*—upregulated genes, *blue*—downregulated genes. *Vertical lines* represent cut-off values for $\log_2$(Fold change): 1 and −1. *D*, enrichment map with GO terms that were significantly upregulated (*red*) or downregulated (*blue*) upon 102×PR expression (FDR q-value < 0.1) and grouped into the following clusters. Color intensity is proportional to the normalized enrichment score (NES) for a given GO term. Node size is proportional to a total number of genes in GO category (gene set size). *E*, heat maps with Z-scores for selected genes from various stress pathways (RQC—ribosome quality control, ISR—integrated stress response, UPR—unfolded protein response) in cells with induced expression of ChFP, poly-K coded by (AAA) codons or 102×PR. *Arrows* indicate differentially expressed genes (*up/down arrows* for upregulated and downregulated genes, respectively) in cells with induced staller expression when compared to ChFP-expressing cells. ChFP, mcherry fluorescent protein; GFP, green fluorescent protein.

clustered separately to all the other sample groups as well as the cells that were uninduced (Fig. 3*B*). Volcano plots revealed that expression of polyadenosine led to relatively minor changes in gene expression, whereas 102×PR expression led to substantial changes (Fig. 3*C*). Indeed, 102×PR expression resulted in 9962 genes significantly changing expression compared to cells expressing ChFP. Of these, 5086 genes were significantly upregulated and of these 1037 more than 2-fold. Four thousand eight hundred and seventy-six genes were significantly downregulated and of these 647 genes by more than 2-fold (Additional File 2). For the poly-K staller, 303 genes were significantly upregulated, but none more than 2-fold. One hundred and two genes were downregulated, and of these, only two showed more than a 2-fold decrease.

Gene set enrichment analysis identified 170 Gene Ontology (GO) terms that were significantly upregulated in the 102×PR-expressing cells and 327 GO terms that were downregulated (Additional File 2). Further pathway enrichment analysis (Additional File 4: Fig. S4) revealed that many GO terms related to ribosome biogenesis, RNA metabolism, RNA processing, RNA transport, and RNA modification (mostly methylation) were upregulated in response to 102×PR expression (Fig. 3*D*). It has been reported that the expression of poly-PR inhibits global translation possibly due to interactions of poly-PR with ribosomes and other components of the translation machinery (26–28).

Polysome profiling revealed 102×PR co-eluted with fractions containing polysomes, unlike GFP and poly-K (Additional File 4: Fig. S5). These data are consistent with the stalled poly-PR protein being multivalently bound to ribosomes or leading to unresolved ribosome stalls, whereas in the case of poly-K, the stalls are efficiently resolved to liberate the free ribosome subunits. As such, our results may reflect a compensatory response to activate genes involved in global translation. Other upregulated GO terms were linked to cytoskeleton which is in the agreement with prior findings of poly-PR disturbing the organization of the cytoskeleton (29) and interacting with actin-related cytoskeletal proteins (17). Our data also support the role for poly-PR in inhibiting DNA double strand break repair pathways (30) as we saw an upregulation of GO terms related to mitotic cell cycle such as negative regulation of nuclear division (GO:0051784), negative regulation of metaphase/anaphase transition of cell cycle (GO:1902100), negative regulation of chromosome organization (GO:2001251), and mitotic intra-S DNA damage checkpoint signaling (GO:0031573).

In addition, many metabolic pathways were downregulated as a result of 102×PR expression. Prominent were clusters of GO terms related to glycoprotein metabolism, lipid biosynthesis, and other terms related to cellular metabolic processes. These findings suggested there was a substantial metabolic adaptation to the 102×PR expression. This result is consistent with previous reports finding that poly-PR directs promiscuous proteome binding and cytotoxicity (17, 27). The other point of note was the significant upregulation of RQC-associated genes as well as some genes involved in integrated stress response (Fig. 3*E*). These effects were not seen with the poly-K construct. This finding suggested that stalling of poly-K coded by polyadenosine can be readily accommodated by proteins that already present in cell whereas 102×PR stalled complexes are more detrimental to cell health and require a massive stress response from a cell.

Genome-wide knockout screen unmasks a distinct signature of regulators of 102×PR readthrough compared to poly-K readthrough

To investigate whether mechanisms that are known to regulate stalls on polyadenosine mRNA are involved in sensing and responding to poly-PR stalls, we performed a genome-wide CRISPR/Cas9 knockout screen using the Brunello library, which targets 19,114 human genes at a coverage of four sgRNA targets per gene (31). We performed two screens: one with the 102×PR staller reporter and the other with poly-K coded by (AAA) codons as a reference for known RQC regulatory mechanisms (22, 32, 33). Flow cytometry was used to sort and collect two groups of cells reflecting the higher and lower 5% ranges of ChFP/GFP ratios (Fig. 4*A*). Population "H" represented cells with the highest ChFP/GFP ratio which should encompass the highest readthrough levels. Population "L" represented cells with the lowest ChFP/GFP ratio, *i.e.*, cells with most stalling events. The logic of the screen was that if a particular gene pauses translation on the studied sequence or recruits quality control machinery to stalled ribosomes, the depletion of this gene would reduce stalling (*i.e.*, cells with this knockout will be over-represented in the H population). Conversely, knockouts of genes stabilizing translation on staller sequences would be enriched in the L population which depicts the lowest levels of readthrough.

The poly-K screen yielded 96 gene knockouts enriched in population H (of these 19 were enriched more than 2-fold), and 56 gene knockouts enriched in population L (and of these 26 were by more than 2-fold) (Fig. 4*B* and Additional File 3). The 102×PR screen yielded 34 gene knockouts enriched in population H (and of these 5 were by more than 2-fold) and 43 gene knockouts enriched in population L (and of these 15 were by more than 2-fold). Twenty-one gene knockouts were observed in common for both screens that increased apparent readthrough (H), and there were 12 genes in common that appeared to increase stalling (L). Fig. 4*C* shows a further refined list of top gene knockouts for each staller which consists of gene knockouts that were significantly enriched in one population (false discovery rate [FDR] < 0.05, log2 fold change [LFC] > 0) and simultaneously depleted from the opposite population (FDR < 0.05, LFC < 0).

The genes found in the poly-K screen included *ZNF598*, a previously known activator of the RQC (21), and members of ASC-1 complex (*ASCC3*, *ASCC2*, and *TRIP4*) that disassembles collided ribosomes that result from stalling on polyadenosine mRNA (34) (Table 1). These knockouts were enriched in population H, which is consistent with other studies showing their knockout to improve poly-K readthrough (21, 22, 34). Another gene involved in RQC activation, *RACK1* (22), also appeared in our screen. Cells with *RACK1* knockout were significantly depleted from population L and

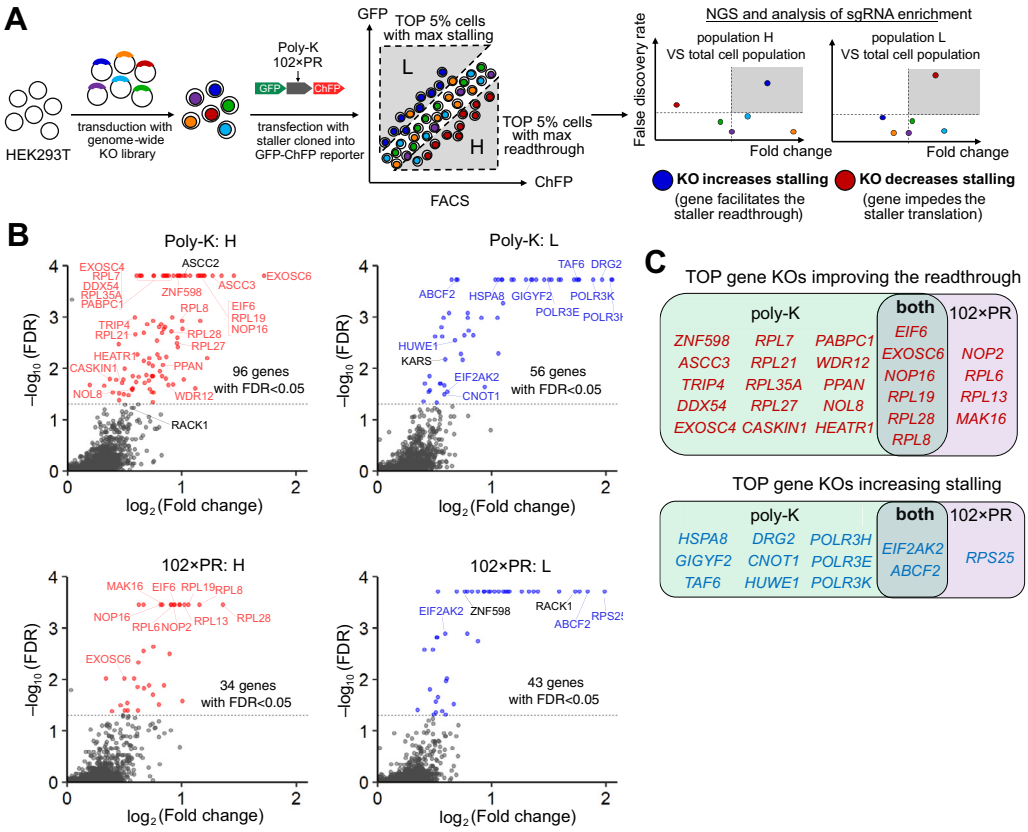

Figure 4. Genome-wide knockout screening for genes modulating stalling of poly-K and poly-PR stallers. *A*, schematic of strategy. *B*, volcano plots of gene KO enrichment. The number on the plot indicates the number of screen hits (FDR < 0.05) for each category. Genes targeted by the sgRNAs that were enriched in population H (highest ChFP/GFP ratio) are shown in *red*. Genes targeted by sgRNAs that were enriched in population L (lowest ChFP/GFP ratio) are shown in *blue*. *C*, *top* screen hits for each staller (*red* – KOs causing readthrough, *blue* – KOs increasing stalling). Genes in *bold* indicate genes that appeared as TOP screen hits for both stallers. ChFP, mcherry fluorescent protein; FDR, false discovery rate; GFP, green fluorescent protein.

on the threshold for significant enrichment in population H (an FDR value of 0.059). Collectively, these findings provided confidence in the screen for finding the relevant genes involved in sensing and resolving stalled ribosomes. It was previously shown that EIF4E2-GIGYF2 (also known as 4EHP-GIGYF2) complex represses translation on defective mRNAs (35) and is recruited to ribosome collisions along with ZNF598 (36). According to our screen, cells with *EIF4E2* and *GIGYF2* knockouts appeared to have more stalling with the poly-K staller. This finding supports the hypothesis that in the absence of EIF4E2-GIGYF2 complex, ZNF598 function on polyadenosine mRNA is enhanced.

Genes known to be involved in activating the RQC showed a distinct enrichment pattern in the 102×PR screen (Table 1). Notably, cells with *ZNF598* and *RACK1* knockouts were enriched in population L which is the opposite to what we observed for poly-K staller. *ASCC3*, *ASCC2*, and *TRIP4* knockouts showed no enrichment in the 102×PR screen despite being hits in the poly-K screen. Other known ribosome rescue factors that can dissociate elongation complexes stalled at the 3′ end of mRNA (*HBS1L*, *PELOTA*, and *ABCE1*) (37), interact with ribosome collisions (*EIF4E2*, *GIGYF2*), or rescue ribosomes stalled at AGA arginine codons (*GTPBP1*, *GTPBP2*) (38) were not enriched in the 102×PR screen. These results suggested that cotranslation and ribosome-associated quality control mechanisms that recognize stalled ribosomes on polyadenosine sequences or other defective mRNAs might be unable to perform this function for poly-PR-induced stalls.

For further clues to pathways associated with genes identified in our screen we performed functional enrichment analysis. For both polyadenosine and poly-PR, GO terms related to translation were enriched among gene knockouts improving the readthrough (Fig. 5, *A* and *B*). These are consistent with the key role of global translation since interference with translation strongly impacted the stall reporter behavior in our screen. This finding is supported by prior work in yeast showing that deletion of ribosomal proteins increases readthrough of poly-K and no-go decay reporters (13). Knockouts of elongator complex (*ELP3*, *ELP4*, and *ELP5*) and thiouridylase *CTU1*, which are required to efficiently decode AAA repeats by modifying U34 of lysyl-tRNA(UUU) (39), decreased the readthrough of poly-K. In addition, deletion of lysyl-tRNA synthetase (*KARS*) which catalyzes the formation of Lys-tRNA^{Lys} selectively increased stalling on poly-K, but not on 102×PR staller which lacks Lys codons. The identification of these genes and pathways provides further evidence that our screen can identify modifiers of translation on staller sequences. Of note, genes activating RQC were identified in both screens, yet the genes showed different enrichment patterns

Table 1
Enrichment factors for genes involved in rescue of stalled ribosomes

Gene name	Gene function	Poly-K					102×PR				
		H: high ChFP/GFP		L: low ChFP/GFP		Effect of gene KO[a]	H: high ChFP/GFP		L: low ChFP/GFP		Effect of gene KO
		FDR[b]	LFC[c]	FDR	LFC		FDR	LFC	FDR	LFC	
ZNF598	Ubiquitin-ligase, recognizes ribosome collisions and targets them for ASC-1 complex and RQC (69)	2E-04	0.98	8E-04	−1.35	read	0.69	−0.28	2E-04	0.76	stall
RACK1	Component of the 40S subunit, facilitates activation of RQC on collided ribosomes (22)	0.059	0.56	8E-04	−1.79	read	0.08	−0.65	2E-04	1.73	stall
ASCC3	Helicase, a member of ASC-1 complex that disassembles collided ribosomes (34, 70)	2E-04	1.27	3E-03	−1.58	read	1	−0.13	0.43	0.55	–
ASCC2	Ubiquitin-binding protein, a member of ASC-1 complex that disassembles collided ribosomes (70)	2E-04	1.02	0.48	−0.46	read	1	0.11	0.99	0.22	–
TRIP4	A member of ASC-1 complex that disassembles collided ribosomes, suggested to promote binding of ASC-1 complex to ribosome (70)	1E-03	0.59	2E-03	−1.26	read	0.95	−0.19	0.17	0.40	–
EIF4E2	EIF4E2-GIGYF2 (also known as 4EHP-GIGYF2) complex represses translation on defective mRNAs (35) and is recruited to ribosome collisions along with ZNF598 (36)	0.92	0.33	1E-03	1.05	stall	0.99	−0.05	0.75	0.33	–
GIGYF2		0.02	−0.72	2E-04	1.36	stall	0.81	−0.10	0.84	0.31	–
HBS1L	HBS1L-PELO complex in the presence of ABCE1 dissociates ribosomes stalled at the end of a truncated mRNA and therefore lacking mRNA in the A-site (34, 37)	1	−0.07	0.13	−0.41	–	1	0.19	0.79	−0.31	–
PELO		0.69	0.28	0.06	−0.87	–	0.98	0.24	0.87	−0.34	–
ABCE1		1	0.22	1	−0.11	–	1	−0.07	0.79	0.44	–
GTPBP1	Resolve codon-specific ribosome pausing on AGA codons (15, 38)	1	0.16	0.93	−0.24	–	1	0.07	1	−0.05	–
GTPBP2		0.74	0.13	0.70	−0.23	–	0.95	0.29	1	−0.09	–

[a] Effect of gene KO (on stalling): read = KO facilitates readthrough on a staller sequence, stall = KO leads to more stalling on a staller sequence.
[b] False discovery rate.
[c] $\log_2$ fold change.

further supporting our conclusions thus far that the surveillance and quality control mechanisms of stalling is dissimilar between polyadenosine and mRNA encoding 102×PR. Lastly, the enrichment of nuclear transport and nuclear envelope organization genes in 102×PR screen may relate to the recruitment of the poly-PR to the nucleus.

Next, we further examined the role of 14 genes identified in our screen by creating individual knockout cell pools (Fig. 6). These genes were chosen based on their large LFC values in the screen (*DRG2* and *SKIV2L2* for poly-K; *NPM1* and *RPS25* for 102×PR; *ABCF2*, *BOP1*, *DDX27*, *EIF2AK2*, *EIF6*, *NOP2* and *RPL19* for both stallers) or their opposing effects between poly-K and 102×PR stallers (*ZNF598*, *RACK1* and *BANF1*). To understand off-target impacts on the stall reporter readout, we included a linker control construct that contained a sequence known to not induce stalling (20–23) (Table 2). *ZNF598* and *RACK1* have been previously shown to increase readthrough of poly-K coded by (AAA) codons when their levels are reduced (21, 22). Accordingly, their knockout increased the ChFP to GFP ratio by 3.7- and 2.7-fold, respectively, for the poly-K staller. By contrast, both knockouts decreased the ratio for the 102×PR staller, in

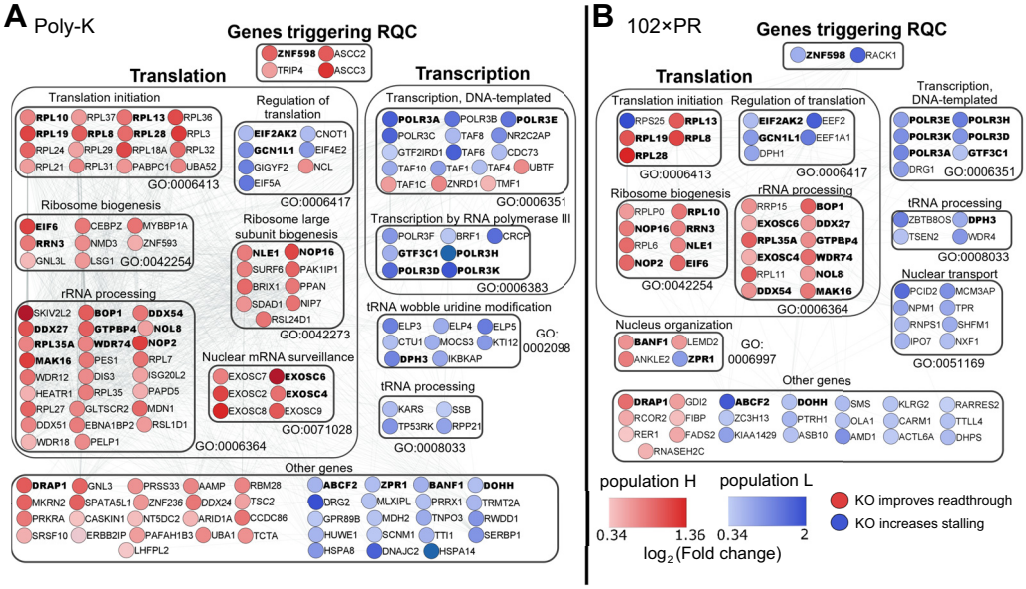

Figure 5. Top enriched gene ontology (GO) terms for screen hits at 5% FDR. *A*, Poly-K. *B*, 102×PR. Genes in *bold* were the screen hits for both stallers. FDR, false discovery rate; RQC, ribosome quality control.

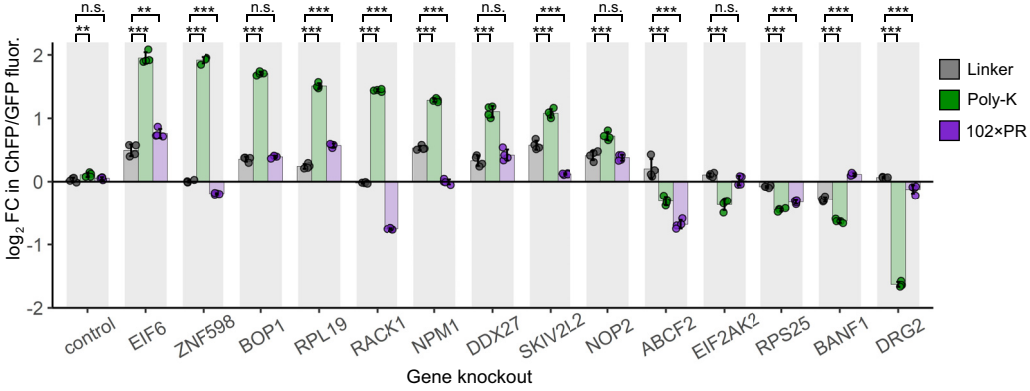

Figure 6. Validation of screen results with individual gene knockouts. Y axis shows $\log_2$ fold changes (LFCs) in ChFP/GFP ratio in HEK293T cells expressing an indicated construct (color legend) after knockout of different genes selected from our screen hits. Control—cells expressing nontargeting sgRNA. Data represents means, bars show SD, n = 4. LFCs for each staller were compared to LFC for a linker construct using one-way ANOVA and Dunnett's post hoc test. n.s. – not significant; $^{**}p < 0.01$; $^{***}p < 0.0001$. ChFP, mcherry fluorescent protein; GFP, green fluorescent protein.

agreement with the screen outcomes which indicated that stalling was more pronounced when these genes are depleted. Most of the knockouts that increased ChFP/GFP ratio on 102×PR staller (*BOP1, DDX27, NOP2*) had the same impact on linker control suggesting that observed effects were not specific to 102×PR translation (Fig. 6). Other genes knockouts that impacted ChFP/GFP ratio on poly-K staller mostly had negligible or small effects on 102×PR readthrough except for *ABCF2*. By measuring ChFP/GFP ratios at different levels of GFP fluorescence, we confirmed that the observed effects of gene perturbation on staller readthrough are consistent across the whole range of staller expression (Additional File 4: Fig. S6). Collectively, these results are consistent with the surveillance mechanisms involved in sensing stalls on polyadenosine mRNA having minimal if any impact on 102×PR elongation efficiency even if they may be able to sense such translation events as problematic based on their upregulation in the RNA-seq data.

We also examined whether these genes displayed similar effects with 102×GR, which stalls more severely than 102×PR. None of the gene knockouts had any major effects on the ChFP/GFP ratio, suggesting that the stalling behaves similarly to that of 102×PR (Additional File 4: Fig. S7). However, the two knockouts that worsened stalling for 102×PR (*RACK1* or *ABCF2*) appeared to have no effect on 102×GR. This may be explained by the finding that 102×GR is more substantially stalled than 102×PR and hence has no capability to be further stalled (17) (Fig. 1, *B* and *C*).

Table 2
Validation of screen hits by individual knockouts

		KO effect on staller readthrough					
		In screen[a]		Individual KO cell pool, compared to control cells[b]		Individual KO cell pool, compared to linker[c]	
Gene	Function	Poly-K	102×PR	Poly-K	102×PR	Poly-K	102×PR
ABCF2	Unknown, a member of ABC transporters family	stall	stall	stall***	stall***	stall***	stall***
BANF1	Nuclear assembly and chromatin organization (71)	stall	read	stall***	n.s.	stall***	read***
BOP1	60S ribosome subunit biogenesis (72)	read	read	read***	read***	read***	n.s.
DDX27	RNA helicase involved in rRNA processing (73)	read	read	read***	read***	read***	n.s.
DRG2	Unknown, important role in cell growth (74)	stall	n.s.	stall***	stall***	stall***	stall***
EIF2AK2	(Also: PKR) inhibits cellular translation during stress (75)	stall	stall	stall***	n.s.	stall***	n.s.
EIF6	Ribosome biogenesis, binds to 60S to prevent premature association with 40S subunit (76)	read	read	read***	read***	read***	read**
NOP2	Nucleolar maturation and ribosome biogenesis (77)	read	read	read***	read***	read***	n.s.
NPM1	RNA transport and ribosome biogenesis (78)	n.s.	stall	read***	n.s.	read***	stall***
RACK1	Scaffolding protein, component of 40S ribosome; activator of RQC on polyadenosine mRNA (22)	n.s.	stall	read***	stall***	read***	stall***
RPL19	60S ribosomal protein	read	read	read***	read***	read***	read***
RPS25	40S ribosomal protein, required for efficient RAN translation of C9orf72 repeats (79)	n.s.	stall	stall***	stall***	stall***	stall***
SKIV2L2	(Also: MTREX) RNA helicase, associated with the RNA exosome complex (80)	read	n.s.	read***	n.s.	read***	stall***
ZNF598	Activator of RQC on polyadenosine mRNA (21)	read	stall	read***	stall***	read***	stall***

[a] Based on the screen results, read = significantly enriched in H population, stall = significantly enriched in L population.
[b] Shows the KO effect on a staller readthrough. Comparisons were made between different cell lines expressing a given staller: KO cell pool *versus* control cell pool (cells with nontargeting sgRNA).
[c] Shows if the KO effect on staller is significantly different from the KO effect on a linker readthrough. Comparisons were made within a given KO pool, between cells expressing an indicated staller and cells expressing linker control.
[b,c] Comparisons were made between $\log_2$ fold changes (LFC) in ChFP/GFP. For each knockout, LFC = $\log_2$(the ratio in cells with sgRNA targeting an indicated gene divided by the ratio in non-infected cells without sgRNA). n.s. – not significant; $^{**}p < 0.01$; $^{***}p < 0.0001$, as determined by one-way ANOVA and Dunnett's post hoc test (n = 4).

Inhibiting global translation increases the readthrough of poly-K, but has limited effect on R-rich DPR translation

While elongation of R-rich DPR-coding sequences remained mostly unaffected by various genetic perturbations, we did note that *EIF6* and *RPL19* knockouts yielded slightly increased ChFP/GFP ratios for 102×PR staller relative to linker control (Fig. 6). eIF6 is a translation initiation factor that binds 60S ribosomal subunits and prevents 60S from prematurely joining 40S subunits. Reduction of eIF6 levels causes a decrease in available 60S subunits and impairs protein synthesis (40). To test whether reducing the ribosome load and translational throughput on mRNA can improve the elongation efficiency of R-rich DPRs, we performed an experiment modeled on prior experiments showing that reducing the number of ribosomal collisions increases protein output from some stall sequences and stabilizes their translation (13). For this, we applied low concentrations of translation initiation inhibitor harringtonine to reduce the density of ribosomes on mRNAs (41). As anticipated for a collision-based mechanism of stalling, harringtonine treatment led to a considerable increase in ChFP/GFP ratio for poly-K staller (up to 3.5-fold). Low doses of harringtonine had a more modest effect on 102×PR and almost no effect on 102×GR staller (Fig. 7, *A* and *B*). The effect of harringtonine was more pronounced in cells with lower expression of constructs (Additional File 4: Fig. S6). Collectively the findings suggest that when the density of ribosomes on mRNA transcripts is reduced, there is a capacity for a small improvement in stalling for the Arg-rich DPRs. However, whether mechanisms are involved to clear this remains to be determined as they do not appear to be effectively managed by the known RQC genes.

Discussion

Collectively, our findings show that ribosomes cannot efficiently translate long R-rich DPRs due to a stalling effect and that the stalling mechanism appears ineffectively managed by

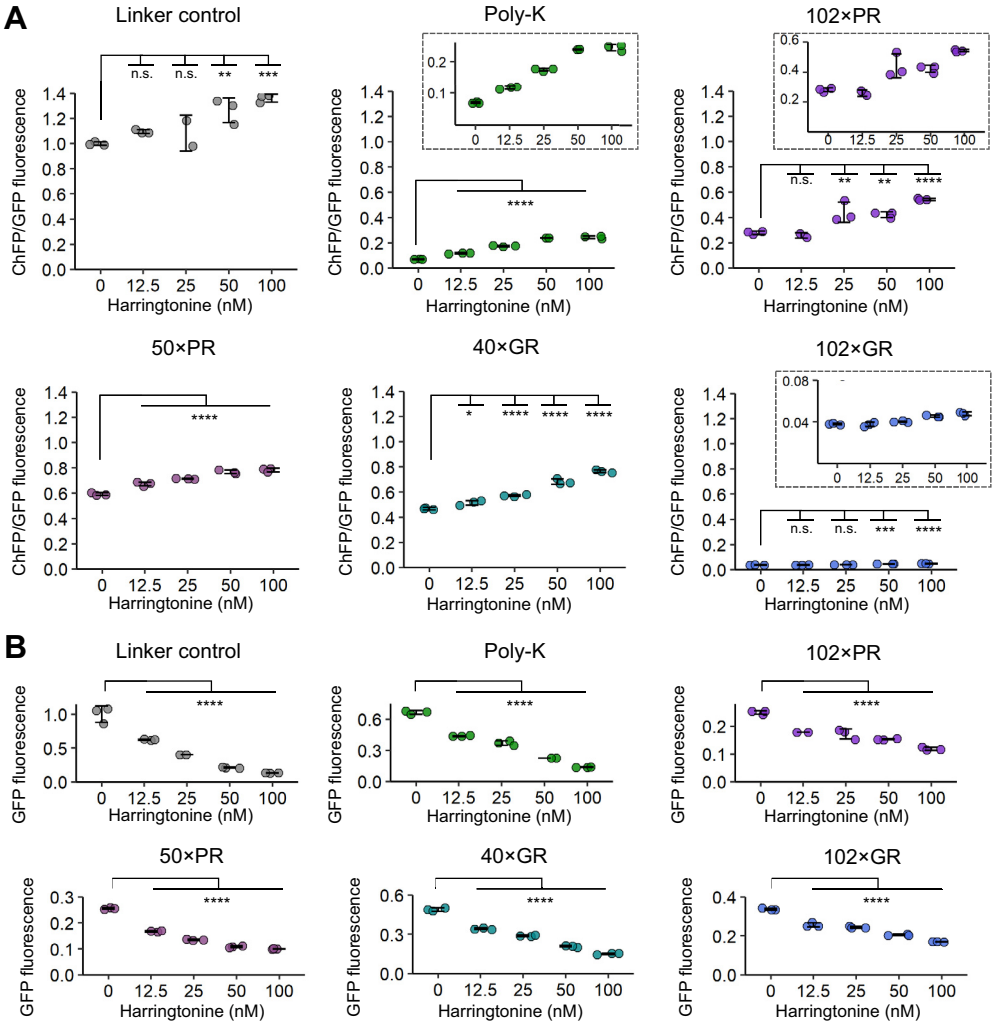

Figure 7. The effect of translation inhibition on the readthrough of various R-rich DPRs. HEK293T cells were transfected with different fluorescent stall reporters, and various concentrations of translation inhibitor harringtonine were added 6 h after transfection before visible formation of fluorescent proteins. Cells were subjected to FACS after 18 h of treatment with harringtonine. *A*, relative ChFP/GFP ratios in cells expressing different constructs and treated with indicated concentration of translation inhibitor. *B*, relative GFP median fluorescence intensities for the data shown in panel A. Relative ChFP/GFP ratios and GFP levels were calculated by normalizing to linker control (set as 1). Data represents means, error bars show SD, n = 3. n.s. – not significant; *$p < 0.05$, **$p < 0.01$, ***$p < 0.001$, ****$p < 0.0001$ as determined by one-way ANOVA and Dunnett's post hoc test. ChFP, mcherry fluorescent protein; GFP, green fluorescent protein.

established quality control mechanisms. The polysome profiling data points to the 102×PR binding to polysomes, which is consistent with large multivalent interactions mediated by the Arg being involved in aggregating the translational machinery (27). Whether dipeptide-induced ribosome pausing is critical here to ribosome collision, as opposed to a more nonspecific aggregation of polysomes remains to be determined by structural and other studies. The findings are broadly in line with previous findings that R-rich DPRs are promiscuous interactors to other cellular proteins including actin (17). As such stalling may be one mechanism of many that simultaneously drive dysfunction and the profound transcriptional signatures of stress and metabolic changes.

Previous studies have shown that unresolved ribosome stalling leads to cell cycle arrest (17), suggesting this mechanism is potentially important in the cascade of neurodegeneration. A recent study found that aging, which is accompanied by a decline in cellular proteostasis, causes greater ribosome pausing at polybasic stretches (42). If high linear densities of charged amino acid sequences in nascent chains require greater demand on mechanisms to resolve pauses or stalls, then aging and/or the presence of other stresses may provide a temporal and age-dependent trigger for Arg-rich DPR–mediated toxicity in disease onset and development.

While our knockout screen did not appear to identify novel regulatory mechanisms for regulating Arg-rich DPR stalling, when we slowed translation initiation with harringtonine, we observed a small improvement in readthrough. This finding raised the possibility that there are undiscovered mechanisms that can aid the resolution of Arg-rich DPR stalls or that RQC can work to resolve such stalls but much less effectively than for polyadenylate sequences. Indeed, a recent study found that a key protein of the RQC, ZNF598, reduced synthetic poly-GR cytotoxicity in human neuroblastoma cells when overexpressed (18). Further, this study identified a missense mutation in an ALS patient from a large-scale whole-genome sequencing study in ALS (43), ZNF598R69C, that failed to show any beneficial role when overexpressed suggesting that the clearance mechanisms related to RQC are ALS-relevant.

Based on the 40×Gly-Xxx DPR screen, we find that elongation efficiency is consistently reduced in 16 out of 19 amino acids compared to the nonstall linker control with only Phe not being significantly different and Tyr and Val seemingly increasing the readthrough. Of these 16, apart from Trp, Arg, Asp, Glu, and Lys, the ratio was about 75% of that of the linker, which may reflect a contributory effect of Gly on stalling or potentially differences in the length of amino acids between the linker construct (which has 120 amino acids) and the 40×DPRs (approx. 80 amino acids). Of those that changed the ratios substantially, the charged amino acids were all potent stallers (Arg, Lys, Glu, and Asp), suggesting that a high linear density of charged amino acids in the repeat sequence is sufficient to suppress translation irrespective of whether that is a positive or negative charge. Also of note was the potent translation suppression by Trp. It is plausible that this effect arises from a low availability of tryptophanyl-tRNA^{Trp} (44) and/or the high energy cost of its biosynthesis (45, 46). The reason why Tyr and Val increased the readthrough, and indeed Phe being above the other 16 amino acids, is unclear.

Another question that remains unsolved is the mechanism by which Arg-rich DPR stalls occur. Simulations have suggested that positively charged residues in the nascent chain generate mechanical forces that pull the A- and P-sites away from each other which distorts the configuration of the peptidyl transferase center and increases the free energy barrier for the peptide bond formation (47, 48). The ribosome exit tunnel can hold about 30 amino acids of a linear peptide chain and up to 60 amino acids for a peptide in an α-helical conformation (49). R-rich DPRs require more than 10 repeats (*i.e.*, 20 amino acids for the poly-GR) and up to 40 repeats (80 amino acids for the poly-PR) to cause small levels of stalling (*i.e.*, 25% or less). Such lengths would be sufficient to fill the ribosome exit tunnel and stall through an electrostatic jamming mechanism as previously proposed (17–19). However, longer dipeptide lengths (>40 repeats for poly-GR (80 amino acids) and >50 repeats for poly-PR (100 amino acids)) are required to stall more than 50%. The readthrough of sequences that encode poly-GR or poly-PR by the ribosome decreases in a length-dependent manner suggesting that emergent DPR chain is involved in stalling. This effect may be part of a more promiscuous pattern of nonselective interactions drive by the high linear density of arginine. A recent study suggested that the addition of short synthetic 20×PR and 20×GR polypeptides strongly inhibited global translation *in vitro* and occluded the exit tunnel of eukaryotic 80S ribosomes (19). Accordingly, it is reasonable to predict that during R-rich DPR translation, emergent poly-GR or poly-PR nascent chains could bind and block the exit tunnels of trailing ribosomes on the mRNA leading to obstruction of translation in trans and a collateral aggregation of translational machinery. The support to this mechanism comes from poly-GR and poly-PR interactomes being enriched with translational proteins (17, 27) and our data herein showing poly-PR to be associated with polysomes. A further twist to this mechanism comes from simulations suggesting that the R-rich DPRs can phase separate once they reach a polymer length of about 25 repeats (50). Hence translation may be inhibited through a coalescence of ribosomes and blockage of their exit tunnels, which would presumably confer a great deal of toxic stress to cellular functioning.

Another aspect to our data is why the poly-GR appears to be more potent at stalling than poly-PR. One possibility is that the glycine allows greater conformational flexibility than proline (50). One consequence is that it may allow compact structures to accumulate in the ribosome exit tunnel, which may exacerbate blockage through electrostatic interactions. Indeed, the exit tunnel is wide enough to allow small protein domains to fold before exiting the ribosome tunnel (51). A greater flexibility may also lend to greater potency in influencing ribosomes in trans.

Poly-PR expression invokes a profound transcriptional response from cells compared to poly-K expression, including genes involved in translation and cytoskeleton. Some of these

responses likely arise from the multipronged toxicity previously implicated from poly-PR, including inhibition of translation (26–28) and the disruption of cytoskeleton architecture (17, 29, 52). Other responses relate to stress response pathways, which may be secondary to multipronged effects of poly-PR. However the strong involvement of RQC genes suggests that some cellular mechanisms respond to the presence of DPR stalled complexes even if these mechanisms may be poorly adapted to clearing them. Indeed other work has pointed to a role for RQC activator protein ZNF598 promoting the cleavage of poly-GR (but not poly-PR) by the ubiquitin-proteasome system while not affecting the readthrough efficiency (18). As such, the stalling may simply be overwhelming or improperly sensed by machinery that has not evolved to deal with such unnatural stalling sequences. In turn, it is plausible that the other stress responses are invoked in response to that inability to resolve through the RQC. Of note are studies finding DPR deposits in brain tissue to correlate with markers of the unfolded protein response (53).

In conclusion, our study provided evidence for the Arg-rich DPRs causing a unique mechanism of stalling that existing cellular responses, including the RQC, seem poorly equipped to processing for resolution.

Experimental procedures

DNA constructs

Plasmids coding the linker, poly-K, 102×GR, and 102×PR (the number in front of amino acid pair indicates the number of DPRs, *e.g.*, 102×GR; this nomenclature was interchangeably described as $(GR)_{102}$) in dual fluorescence stall reporter were prepared as described (17). Poly-K refers to a AAA repeat of 21 length; and ChFP refers to the mCherry fluorescent protein. cDNA for 20×, 30×, 40×, 50×, 75×GR and PR, and 40×GA, GC, GD, GE, GF, GH, GI, GK, GL, GM, GN, GP, GQ, GS, GT, GV, GW, GY were synthesized and cloned into dual fluorescence stall reporter (GenScript). SOD1(A4V)-ChFP was generated as described (54). For knockout cell pools, sgRNA sequences targeting genes of interest were designed using Benchling software. They were cloned into lentiCRISPRv2 vector (a gift from Feng Zhang; Addgene plasmid # 52961) (55) using BsmBI restriction sites, as outlined in the protocol from Zhang lab (available at Addgene). For stable Tet-inducible cell lines, GFP-P2A-ChFP, GFP-P2A-poly-K, and GFP-P2A-102×PR were cloned by restriction digestion and ligation and inserted into pLVX-TetOne-Puro vector (Takara Bio # 631849) using Gibson assembly. For sucrose density gradient fractionation, pEGFP-C2 vector was used for thew expression of GFP, GFP-poly-K or GFP-102×PR (poly-K or 102×PR sequences were added to the C-end of GFP *via* restriction cloning). All cloned constructs were validated by sequencing. DNA preparations were made with Stbl3 *Escherichia coli* cells (Thermo Fisher). The sequence information is available (Additional File 1).

Cell culture

HEK293T cells, obtained originally from the American Type Culture Collection (ATCC), were maintained in complete Dulbecco's modified Eagle medium (DMEM) supplemented with 10% v/v fetal calf serum and 1% GlutaMAX. Cells were cultured in a humidified incubator with 5% v/v atmospheric CO_2 at 37 °C. For the drug treatment experiments, harringtonine (Abcam # ab141941; 20 mM working stock in DMSO) was added to cells 6 h posttransfection alongside a change of culture medium, and cells were analyzed by FACS at 24 h posttransfection.

Ribosomal stalling assays

HEK293T cells were transfected with staller constructs using Lipofectamine 3000 reagent and harvested 24 h posttransfection. Cells were analyzed using LSRFortessa X-20 flow cytometer (BD Biosciences). Side and forward scatter height, width, and area were collected to gate for single live cell population. GFP fluorescence was collected with the 488-nm laser and FITC (530/30) filter to gate for transfected cells, ChFP fluorescence was collected with the 561-nm laser and ChFP (610/20) filter. Flow cytometric gating and data analysis was performed using FlowJo software (v10.5.3), and graphs were analyzed in RStudio (v. 1.4.1106) and GraphPad Prism 8. Median FITC-A and median ChFP-A fluorescence intensities were used to calculate ChFP/GFP ratios. All ratios were normalized to the average ChFP/GFP ratio for fluorescence reporter containing control linker sequence (set as 1).

Western blot

Cells were pelleted by centrifugation at 120*g* for 6 min and resuspended in RIPA buffer for lysis and incubated at 4 °C for 10 min. Protein concentration was determined by BCA, matched across samples, and then run on SDS-PAGE followed by transfer using iBlot2. The membrane was blocked with 5% (w/v) skim milk in PBS-T for 1 h at room temperature followed by an incubation in either anti-GFP (Invitrogen # A-6455, 1:5000) or anti-Cherry antibody (Abcam # ab167453, 1:5000) in PBS-T for 1 h at room temperature. The blots were washed in PBS-T and then incubated with anti-rabbit secondary antibody (Invitrogen # 65–6120, 1:20,000) in PBS-T for 1 h at room temperature. Proteins were detected by an enhanced chemiluminescence kit (Clarity, Bio-Rad).

Lentiviral work

Lentivirus for Brunello knockout library, single knockout cell lines, and Tet-inducible cell lines were made per Thermo Fisher guidelines with minor modifications. HEK293T cells were transfected with pCMV-VSV-G (a gift from Bob Weinberg; Addgene plasmid # 8454) (56), psPAX2 (a gift from Didier Trono; Addgene plasmid # 12260), and lentiviral transfer plasmid in equimolar ratios using Lipofectamine 3000 reagent. Virus-containing media were collected 48 h posttransfection and filtered using 0.45 μm filter. Virus supernatant was stored at −80 °C. HEK293T cells were transduced with virus in the presence of 8 μg/ml polybrene. The media were refreshed with complete DMEM 24 h after transduction. At 48 h after transduction, antibiotic selection for infected cells were performed with 1 μg/ml puromycin

(Thermo Fisher # A1113803; 10 mg/ml working stock in 20 mM HEPES buffer) for 3 days.

RNA sequencing

Using lentivirus, we created three stable HEK293T cell lines expressing GFP-P2A-ChFP (negative control), GFP-P2A-poly-K, and GFP-P2A-102×PR under a Tet-inducible promoter. Expression was induced by adding complete DMEM media containing 500 ng/μl doxycycline (Sigma-Aldrich # D9891; 1 mg/ml working stock in DMSO); in parallel, DMEM containing equal concentration of DMSO was added to uninduced cells. Expression was confirmed in the induced samples by microscopy and flow cytometry for the fluorescent proteins. After 48 h of induction, cells were washed with PBS and then collected in ice-cold 20 mM Tris pH 7.4, 150 mM NaCl, 5 mM $MgCl_2$, 1 mM DTT, 100 μg/ml cycloheximide, 1% v/v Triton X-100, and 25 U/ml Turbo DNase I, with a cell scraper. For each construct, uninduced cells were collected in parallel to the doxycycline-induced cells. After incubation for 10 min on ice, lysed cells were triturated 10 times through a 26-gauge needle and centrifuged for 10 min at 20,000*g* at 4 °C. The RNA concentration in the supernatant was measured using Promega QuantiFluor RNA System. Total RNA was isolated by Zymo Research Direct-zol RNA MiniPrep Kit from lysate containing 30 ug of RNA. The stranded mRNA library was prepared using TruSeq mRNA Library Prep with polyA selection. Libraries were sequenced on the Illumina NovaSeq 6000 (100 bp Single Read, 20M reads per sample) by the Australian Genome Research Facility. Real Time Analysis (RTA) v.3.4.4 was used for basecalling, and then, the Illumina bcl2fastq 2.20.0.422 pipeline was used to generate the sequence data. All samples were prepared in triplicates.

Sucrose density-gradient fractionation

Polysome profiling analysis was performed as described in (57). HEK293T cells transfected with GFP, GFP-poly-K, or GFP-102×PR were incubated with 100 μg/ml of cycloheximide (Sigma-Aldrich # 01810-1G) for 5 min prior to harvest. Cell lysates were clarified by centrifugation and loaded (normalized by OD260) on top of linear 10 to 40% (w/v) sucrose gradients for ultracentrifugation at 222,228*g* for 2¼ h at 4 °C using an SW41Ti rotor (Beckman Coulter). The samples were then fractionated into 1.5 ml tubes with continuous monitoring of UV absorbance at 260 nm by an ISCO UA-6 detector. Individual fractions were analyzed for GFP by dot blotting. 4 μl of each fraction was placed on nitrocellulose membrane and incubated for 1 h until dried. The membrane was blocked in 5% (w/v) skim milk in PBS-T for 1 h at room temperature followed by an incubation in anti-GFP antibody (Invitrogen # A-6455 1:5000) in PBS-T for 1 h at room temperature. The blots were washed in PBS-T and then incubated with anti-rabbit secondary antibody (Invitrogen # 65-6120, 1:20,000) in PBS-T for 1 h at room temperature. Proteins were detected by an enhanced chemiluminescence kit (Clarity, Bio-Rad). GFP fluorescence in fractions 2 to 13 were also measured using Clariostar plate reader. Excitation and emission of 488 nm and 523/10 nm, respectively, was used.

Differential expression and enrichment analysis

Raw sequencing data were processed in Galaxy.org. Reads were trimmed for adaptor sequence using Cutadapt (v.3.4). Trimmed reads were mapped to hg38 human genome using HISAT2 (v.2.1.0) (58). Aligned reads were counted using featureCount tool. Differential gene expression analysis was performed using DESeq2 (v.1.30.1) (59) in RStudio (v. 1.4.1106). The comparisons were made between the following groups of samples: 102×PR.IND *versus* ChFP.IND and poly-K.IND *versus* ChFP.IND; IND = induced. Genes with adjusted p-value < 0.05 were considered as differentially expressed. Gene set enrichment analysis (GSEA) was performed using a javaGSEA desktop application (v.4.1.0) (60, 61), full list of genes with normalized counts generated by DESeq2 (v.1.30.1) was used for the analysis. Curated gene set GSEA: C5.GO.BP.v7.4 was obtained from the Molecular Signatures Database (MSigDB) (62). Datasets with FDR <0.25 were considered as statistically significant. Enrichment map visualization was performed in Cytoscape (v.3.8.0) for all datasets with FDR<0.1 (63). All tables generated from the analysis are available (Additional File 2).

Genome-wide CRISPR/Cas9 knockout screening

The human CRISPR/Cas9 knockout pooled library Brunello was obtained from Addgene (a gift from David Root and John Doench; Addgene # 73178) (31). The experiment was done as outlined in the following protocol (64), with minor modifications. For each of three replicates, HEK293T cells were transduced at multiplicity of infection of 0.4. Following antibiotic selection, at least 100×10^6 cells were transfected with either poly-K or 102×PR. Twenty-four hours posttransfection, half the cells were subjected to sorting while the other half was left as the unsorted population control. Cells were sorted with a BD InFlux cell sorter for the top 5% and bottom 5% of the high and low ChFP/GFP ratio populations, respectively. gDNA from collected cells was extracted with salt precipitation protocol as described previously (65). The sgRNA-containing cassettes were amplified by PCR as described previously (66). The pooled amplicons were sequenced with the Illumina NovaSeq 6000 (100 bp Single Read, 400M reads) by the Australian Genome Research Facility. All samples were prepared in triplicates.

Identification of potential regulators of stalling from CRISPR screen and GO analysis

sgRNA abundances were compared between the following populations: poly-K (H) *versus* polyK.unsorted, poly-K (L) *versus* polyK.unsorted, 102×PR (H) *versus* 102×PR.unsorted, 102×PR (L) *versus* 102×PR.unsorted; H – top 5% high ChFP/GFP ratio population, L – top 5% low ChFP/GFP ratio population, unsorted – control population. Data was analyzed using MAGeCK (v.0.5.9.2) computational tool (67), FDR and

LFC values for each gene were calculated. All genes with FDR<0.05 and positive LFC values meaning they are significantly enriched in one of the sorted populations (H or L) were considered as potential screen hits. Two groups of potential screen hits were generated for each staller: knockouts improving readthrough on staller sequence (enriched in H) and knockouts leading to increased stalling (enriched in L). Top list of screen hits was selected based on significant enrichment in one population (FDR $<$ 0.05, LFC $>$ 0) and simultaneous depletion from the opposite population (FDR $<$ 0.05, LFC $<$ 0) *e.g.*, LFC $>$ 0 in H and LFC $<$ 0 in L. Functional enrichment analysis was done in Cytoscape (v.3.8.0) for all screen hits. All tables generated from the analysis are available (Additional File 3).

Generation of knockout cell pools

Single sgRNA expression vectors were cloned, and lentivirus production with the following transduction was performed as described above. More than 50% knockout efficiency for each pool was validated by ICE-seq analysis (68) after isolating total gDNA and sequencing the targeted region of gene of interest. The sgRNA sequences targeting each selected gene used are shown in Additional File 1. Cells expressing a nontargeting sgRNA were used as a control+ pool. Fold changes in ChFP/GFP ratio for poly-K, 102×PR, or 102×GR after individual gene knockout were calculated by dividing the ratio from cells expressing sgRNA to ratio from cells without sgRNA. For each knockout pool, fold changes in ChFP/GFP on a test sequence were compared against fold changes in ChFP/GFP on a linker sequence that does not cause stalling.

Statistical analysis

Details of quantification including number of samples analyzed are described in the corresponding figure legends and methods section. Plots were made in RStudio (v. 1.4.1106), data are presented as mean ± standard deviation (SD). Statistical tests were performed in GraphPad Prism 8. The Kruskal–Wallis test was performed to identify statistically significant differences in ChFP/GFP ratios between different groups of DPRs (Fig. 2*C*). For all other plots, the means of different groups of samples were compared to control group in GraphPad Prism 8 using one-way ANOVA and Dunnett's post hoc test. p values below 0.05 were considered significantly different. To assess the change in ChFP/GFP ratio after various treatments and gene perturbations across different levels of staller expression (Additional File 4: Fig. S6), the channel values of GFP and ChFP fluorescence were exported from FlowJo (v10.5.3) for each cell from single live transfected gate. Cells were sorted into different bins based on their raw GFP fluorescence intensities (1: GFP $<$ 400; 2: 400 $<$ GFP $<$ 500; 3: 500 $<$ GFP $<$ 600; 4: 600 $<$ GFP $<$ 700; 5: 700 $<$ GFP $<$ 800; 6: 800 $<$ GFP $<$ 900; 7: GFP $>$ 900); only bins with more than 100 cells were left for the analysis. For each bin, ChFP/GFP ratios were calculated and then normalized to linker control (set as 1).

Data availability

RNA sequencing data from this study have been deposited to NCBI GEO with the accession code: GSE193962. All tables generated from the analysis of RNA-seq and CRISPR/Cas9 knockout screening data are available in Additional Files 2 and 3 respectively. All data supporting the findings of this study are available from the corresponding author upon request.

Supporting information—This article contains supporting information.

Author contributions—V. K., L. F., and D. M. H. conceptualization; V. K., A. R. O., E. P. K., H. E. G. M., D. M .H., S. L. A., M. E. R., and L. F. methodology; V. K. validation; V. K. formal analysis; V. K., A. R. O., and E. P. K. investigation; V. K., L. F., and D. M. H. data curation; V. K. and D. M. H. writing—original draft; V. K., A. R. O., and E. P. K. visualization; H. E. G. M. resources; V. K., H. E. G. M., J. D. M., S. L. A., M. E. R., L. F., and D. M. H. writing—review & editing; J. D. M., L. F., and D. M. H. supervision; S. L. A., M. E. R., and H. E. G. M. resources; D. M. H. project administration; D. M. H. funding acquisition.

Funding and additional information—This work was funded by grants to D. M. H. (National Health and Medical Research Council APP1161803 and Australian Research Council DP170103093) and to L. F. [Department of Health and Human Services acting through the Victorian Cancer Agency (fellowship MCRF16007)].

Conflict of interest—The authors declare that they have no conflict of interest with the contents of this article.

Abbreviations—The abbreviations used are: DPR, Dipeptide repeats; RQC, ribosome quality control; DMEM, Dulbecco's modified Eagle medium; FDR, false discovery rate; LFC, $\log_2$ fold change; GFP, green fluorescent protein; ChFP, mCherry fluorescent protein; GO, Gene Ontology; UPR, unfolded protein response.

References

1. DeJesus-Hernandez, M., Mackenzie, I. R., Boeve, B. F., Boxer, A. L., Baker, M., Rutherford, N. J., *et al.* (2011) Expanded GGGGCC hexanucleotide repeat in noncoding region of C9ORF72 causes chromosome 9p-linked FTD and ALS. *Neuron* **72**, 245–256
2. Renton, A. E., Majounie, E., Waite, A., Simon-Sanchez, J., Rollinson, S., Gibbs, J. R., *et al.* (2011) A hexanucleotide repeat expansion in C9ORF72 is the cause of chromosome 9p21-linked ALS-FTD. *Neuron* **72**, 257–268
3. Van Mossevelde, S., van der Zee, J., Cruts, M., and Van Broeckhoven, C. (2017) Relationship between C9orf72 repeat size and clinical phenotype. *Curr. Opin. Genet. Dev.* **44**, 117–124
4. McEachin, Z. T., Parameswaran, J., Raj, N., Bassell, G. J., and Jiang, J. (2020) RNA-mediated toxicity in C9orf72 ALS and FTD. *Neurobiol. Dis.* **145**, 105055
5. Zu, T., Liu, Y., Banez-Coronel, M., Reid, T., Pletnikova, O., Lewis, J., *et al.* (2013) RAN proteins and RNA foci from antisense transcripts in C9ORF72 ALS and frontotemporal dementia. *Proc. Natl. Acad. Sci. U. S. A.* **110**, E4968–E4977
6. Kwon, I., Xiang, S., Kato, M., Wu, L., Theodoropoulos, P., Wang, T., *et al.* (2014) Poly-dipeptides encoded by the C9orf72 repeats bind nucleoli, impede RNA biogenesis, and kill cells. *Science* **345**, 1139–1145
7. Wen, X., Tan, W., Westergard, T., Krishnamurthy, K., Markandaiah, S. S., Shi, Y., *et al.* (2014) Antisense proline-arginine RAN dipeptides linked to C9ORF72-ALS/FTD form toxic nuclear aggregates that initiate *in vitro* and *in vivo* neuronal death. *Neuron* **84**, 1213–1225

8. Mizielinska, S., Gronke, S., Niccoli, T., Ridler, C. E., Clayton, E. L., Devoy, A., *et al.* (2014) C9orf72 repeat expansions cause neurodegeneration in Drosophila through arginine-rich proteins. *Science* **345**, 1192–1194
9. Brandman, O., and Hegde, R. S. (2016) Ribosome-associated protein quality control. *Nat. Struct. Mol. Biol.* **23**, 7–15
10. Joazeiro, C. A. P. (2017) Ribosomal stalling during translation: providing substrates for ribosome-associated protein quality control. *Annu. Rev. Cell Dev. Biol.* **33**, 343–368
11. Collart, M. A., and Weiss, B. (2020) Ribosome pausing, a dangerous necessity for co-translational events. *Nucleic Acids Res.* **48**, 1043–1055
12. Ikeuchi, K., Izawa, T., and Inada, T. (2018) Recent progress on the molecular mechanism of quality controls induced by ribosome stalling. *Front Genet.* **9**, 743
13. Simms, C. L., Yan, L. L., and Zaher, H. S. (2017) Ribosome collision is critical for quality control during No-go decay. *Mol. Cell* **68**, 361–373.e5
14. Sitron, C. S., and Brandman, O. (2020) Detection and degradation of stalled nascent chains via ribosome-associated quality control. *Annu. Rev. Biochem.* **89**, 417–442
15. Ishimura, R., Nagy, G., Dotu, I., Zhou, H., Yang, X. L., Schimmel, P., *et al.* (2014) RNA function. Ribosome stalling induced by mutation of a CNS-specific tRNA causes neurodegeneration. *Science* **345**, 455–459
16. Bengtson, M. H., and Joazeiro, C. A. (2010) Role of a ribosome-associated E3 ubiquitin ligase in protein quality control. *Nature* **467**, 470–473
17. Radwan, M., Ang, C. S., Ormsby, A. R., Cox, D., Daly, J. C., Reid, G. E., *et al.* (2020) Arginine in C9ORF72 Dipolypeptides mediates promiscuous proteome binding and multiple modes of toxicity. *Mol. Cell Proteomics* **19**, 640–654
18. Park, J., Lee, J., Kim, J. H., Lee, J., Park, H., and Lim, C. (2021) ZNF598 co-translationally titrates poly(GR) protein implicated in the pathogenesis of C9ORF72-associated ALS/FTD. *Nucleic Acids Res* **49**, 11294–11311
19. Loveland, A. B., Svidritskiy, E., Susorov, D., Lee, S., Park, A., Zvornicanin, S., *et al.* (2022) Ribosome inhibition by C9ORF72-ALS/FTD-associated poly-PR and poly-GR proteins revealed by cryo-EM. *Nat. Commun.* **13**, 2776
20. Brandman, O., Stewart-Ornstein, J., Wong, D., Larson, A., Williams, C. C., Li, J. W., *et al.* (2012) A ribosome-bound quality control complex triggers degradation of nascent peptides and signals translation stress. *Cell* **151**, 1042–1054
21. Juszkiewicz, S., and Hegde, R. S. (2017) Initiation of quality control during poly(A) translation requires site-specific ribosome ubiquitination. *Mol. Cell* **65**, 743–750.e4
22. Sundaramoorthy, E., Leonard, M., Mak, R., Liao, J., Fulzele, A., and Bennett, E. J. (2017) ZNF598 and RACK1 regulate mammalian ribosome-associated quality control function by mediating regulatory 40S ribosomal ubiquitylation. *Mol. Cell* **65**, 751–760.e4
23. Garzia, A., Jafarnejad, S. M., Meyer, C., Chapat, C., Gogakos, T., Morozov, P., *et al.* (2017) The E3 ubiquitin ligase and RNA-binding protein ZNF598 orchestrates ribosome quality control of premature polyadenylated mRNAs. *Nat. Commun.* **8**, 16056
24. Lin, Y. J., Huang, L. H., and Huang, C. T. (2013) Enhancement of heterologous gene expression in Flammulina velutipes using polycistronic vectors containing a viral 2A cleavage sequence. *PLoS One* **8**, e59099
25. Lu, J., and Deutsch, C. (2008) Electrostatics in the ribosomal tunnel modulate chain elongation rates. *J. Mol. Biol.* **384**, 73–86
26. Lee, K. H., Zhang, P., Kim, H. J., Mitrea, D. M., Sarkar, M., Freibaum, B. D., *et al.* (2016) C9orf72 dipeptide repeats impair the assembly, dynamics, and function of membrane-less organelles. *Cell* **167**, 774–788.e17
27. Hartmann, H., Hornburg, D., Czuppa, M., Bader, J., Michaelsen, M., Farny, D., *et al.* (2018) Proteomics and C9orf72 neuropathology identify ribosomes as poly-GR/PR interactors driving toxicity. *Life Sci. Alliance* **1**, e201800070
28. Moens, T. G., Niccoli, T., Wilson, K. M., Atilano, M. L., Birsa, N., Gittings, L. M., *et al.* (2019) C9orf72 arginine-rich dipeptide proteins interact with ribosomal proteins *in vivo* to induce a toxic translational arrest that is rescued by eIF1A. *Acta Neuropathol.* **137**, 487–500
29. Shiota, T., Nagata, R., Kikuchi, S., Nanaura, H., Matsubayashi, M., Nakanishi, M., *et al.* (2022) C9orf72-derived proline: arginine poly-dipeptides modulate cytoskeleton and mechanical stress response. *Front Cell Dev Biol.* **10**, 750829
30. Andrade, N. S., Ramic, M., Esanov, R., Liu, W., Rybin, M. J., Gaidosh, G., *et al.* (2020) Dipeptide repeat proteins inhibit homology-directed DNA double strand break repair in C9ORF72 ALS/FTD. *Mol. Neurodegener* **15**, 13
31. Doench, J. G., Fusi, N., Sullender, M., Hegde, M., Vaimberg, E. W., Donovan, K. F., *et al.* (2016) Optimized sgRNA design to maximize activity and minimize off-target effects of CRISPR-Cas9. *Nat. Biotechnol.* **34**, 184–191
32. Chandrasekaran, V., Juszkiewicz, S., Choi, J., Puglisi, J. D., Brown, A., Shao, S., *et al.* (2019) Mechanism of ribosome stalling during translation of a poly(A) tail. *Nat. Struct. Mol. Biol.* **26**, 1132–1140
33. Tesina, P., Lessen, L. N., Buschauer, R., Cheng, J., Wu, C. C., Berninghausen, O., *et al.* (2020) Molecular mechanism of translational stalling by inhibitory codon combinations and poly(A) tracts. *EMBO J.* **39**, e103365
34. Juszkiewicz, S., Speldewinde, S. H., Wan, L., Svejstrup, J. Q., and Hegde, R. S. (2020) The ASC-1 complex disassembles collided ribosomes. *Mol. Cell* **79**, 603–614.e8
35. Hickey, K. L., Dickson, K., Cogan, J. Z., Replogle, J. M., Schoof, M., D'Orazio, K. N., *et al.* (2020) GIGYF2 and 4EHP inhibit translation initiation of defective messenger RNAs to assist ribosome-associated quality control. *Mol. Cell* **79**, 950–962.e6
36. Juszkiewicz, S., Slodkowicz, G., Lin, Z., Freire-Pritchett, P., Peak-Chew, S. Y., and Hegde, R. S. (2020) Ribosome collisions trigger cis-acting feedback inhibition of translation initiation. *Elife* **9**, e60038
37. Pisareva, V. P., Skabkin, M. A., Hellen, C. U., Pestova, T. V., and Pisarev, A. V. (2011) Dissociation by pelota, Hbs1 and ABCE1 of mammalian vacant 80S ribosomes and stalled elongation complexes. *EMBO J.* **30**, 1804–1817
38. Terrey, M., Adamson, S. I., Gibson, A. L., Deng, T., Ishimura, R., Chuang, J. H., *et al.* (2020) GTPBP1 resolves paused ribosomes to maintain neuronal homeostasis. *Elife* **9**, e62731
39. Rapino, F., Zhou, Z., Roncero Sanchez, A. M., Joiret, M., Seca, C., El Hachem, N., *et al.* (2021) Wobble tRNA modification and hydrophilic amino acid patterns dictate protein fate. *Nat. Commun.* **12**, 2170
40. Pesce, E., Miluzio, A., Turcano, L., Minici, C., Cirino, D., Calamita, P., *et al.* (2020) Discovery and preliminary characterization of translational modulators that impair the binding of eIF6 to 60S ribosomal subunits. *Cells* **9**, 172
41. Ingolia, N. T., Lareau, L. F., and Weissman, J. S. (2011) Ribosome profiling of mouse embryonic stem cells reveals the complexity and dynamics of mammalian proteomes. *Cell* **147**, 789–802
42. Stein, K. C., Morales-Polanco, F., van der Lienden, J., Rainbolt, T. K., and Frydman, J. (2022) Ageing exacerbates ribosome pausing to disrupt cotranslational proteostasis. *Nature* **601**, 637–642
43. Project MinE ALS Sequencing Consortium. (2018) Project MinE: study design and pilot analyses of a large-scale whole-genome sequencing study in amyotrophic lateral sclerosis. *Eur. J. Hum. Genet.* **26**, 1537–1546
44. Barik, S. (2020) The uniqueness of tryptophan in biology: properties, metabolism, interactions and localization in proteins. *Int. J. Mol. Sci.* **21**, 8776
45. Krick, T., Verstraete, N., Alonso, L. G., Shub, D. A., Ferreiro, D. U., Shub, M., *et al.* (2014) Amino acid metabolism conflicts with protein diversity. *Mol. Biol. Evol.* **31**, 2905–2912
46. Akashi, H., and Gojobori, T. (2002) Metabolic efficiency and amino acid composition in the proteomes of Escherichia coli and Bacillus subtilis. *Proc. Natl. Acad. Sci. U. S. A.* **99**, 3695–3700
47. Leininger, S. E., Rodriguez, J., Vu, Q. V., Jiang, Y., Li, M. S., Deutsch, C., *et al.* (2021) Ribosome elongation kinetics of consecutively charged residues are coupled to electrostatic force. *Biochemistry* **60**, 3223–3235
48. Jiang, Y., and O'Brien, E. P. (2021) Mechanical forces have a range of effects on the rate of ribosome catalyzed peptidyl transfer depending on direction. *J. Phys. Chem. B* **125**, 7128–7136
49. Kramer, G., Boehringer, D., Ban, N., and Bukau, B. (2009) The ribosome as a platform for co-translational processing, folding and targeting of newly synthesized proteins. *Nat. Struct. Mol. Biol.* **16**, 589–597

50. Jafarinia, H., van der Giessen, E., and Onck, P. R. (2020) Phase separation of toxic dipeptide repeat proteins related to C9orf72 ALS/FTD. *Biophys. J.* **119**, 843–851
51. Nilsson, O. B., Hedman, R., Marino, J., Wickles, S., Bischoff, L., Johansson, M., *et al.* (2015) Cotranslational protein folding inside the ribosome exit tunnel. *Cell Rep.* **12**, 1533–1540
52. Fumagalli, L., Young, F. L., Boeynaems, S., De Decker, M., Mehta, A. R., Swijsen, A., *et al.* (2021) C9orf72-derived arginine-containing dipeptide repeats associate with axonal transport machinery and impede microtubule-based motility. *Sci. Adv.* **7**, eabg3013
53. Gami-Patel, P., van Dijken, I., Meeter, L. H., Melhem, S., Morrema, T. H. J., Scheper, W., *et al.* (2021) Unfolded protein response activation in C9orf72 frontotemporal dementia is associated with dipeptide pathology and granulovacuolar degeneration in granule cells. *Brain Pathol.* **31**, 163–173
54. Polling, S., Mok, Y. F., Ramdzan, Y. M., Turner, B. J., Yerbury, J. J., Hill, A. F., *et al.* (2014) Misfolded polyglutamine, polyalanine, and superoxide dismutase 1 aggregate via distinct pathways in the cell. *J. Biol. Chem.* **289**, 6669–6680
55. Sanjana, N. E., Shalem, O., and Zhang, F. (2014) Improved vectors and genome-wide libraries for CRISPR screening. *Nat. Methods* **11**, 783–784
56. Stewart, S. A., Dykxhoorn, D. M., Palliser, D., Mizuno, H., Yu, E. Y., An, D. S., *et al.* (2003) Lentivirus-delivered stable gene silencing by RNAi in primary cells. *RNA* **9**, 493–501
57. Kusnadi, E. P., Trigos, A. S., Cullinane, C., Goode, D. L., Larsson, O., Devlin, J. R., *et al.* (2020) Reprogrammed mRNA translation drives resistance to therapeutic targeting of ribosome biogenesis. *EMBO J.* **39**, e105111
58. Kim, D., Langmead, B., and Salzberg, S. L. (2015) Hisat: a fast spliced aligner with low memory requirements. *Nat. Methods* **12**, 357–360
59. Love, M. I., Huber, W., and Anders, S. (2014) Moderated estimation of fold change and dispersion for RNA-seq data with DESeq2. *Genome Biol.* **15**, 550
60. Subramanian, A., Tamayo, P., Mootha, V. K., Mukherjee, S., Ebert, B. L., Gillette, M. A., *et al.* (2005) Gene set enrichment analysis: a knowledge-based approach for interpreting genome-wide expression profiles. *Proc. Natl. Acad. Sci. U. S. A.* **102**, 15545–15550
61. Mootha, V. K., Lindgren, C. M., Eriksson, K. F., Subramanian, A., Sihag, S., Lehar, J., *et al.* (2003) PGC-1alpha-responsive genes involved in oxidative phosphorylation are coordinately downregulated in human diabetes. *Nat. Genet.* **34**, 267–273
62. Liberzon, A., Birger, C., Thorvaldsdottir, H., Ghandi, M., Mesirov, J. P., and Tamayo, P. (2015) The Molecular Signatures Database (MSigDB) hallmark gene set collection. *Cell Syst.* **1**, 417–425
63. Shannon, P., Markiel, A., Ozier, O., Baliga, N. S., Wang, J. T., Ramage, D., *et al.* (2003) Cytoscape: a software environment for integrated models of biomolecular interaction networks. *Genome Res.* **13**, 2498–2504
64. Joung, J., Konermann, S., Gootenberg, J. S., Abudayyeh, O. O., Platt, R. J., Brigham, M. D., *et al.* (2017) Genome-scale CRISPR-Cas9 knockout and transcriptional activation screening. *Nat. Protoc.* **12**, 828–863
65. Chen, S., Sanjana, N. E., Zheng, K., Shalem, O., Lee, K., Shi, X., *et al.* (2015) Genome-wide CRISPR screen in a mouse model of tumor growth and metastasis. *Cell* **160**, 1246–1260
66. Sanson, K. R., Hanna, R. E., Hegde, M., Donovan, K. F., Strand, C., Sullender, M. E., *et al.* (2018) Optimized libraries for CRISPR-Cas9 genetic screens with multiple modalities. *Nat. Commun.* **9**, 5416
67. Li, W., Xu, H., Xiao, T., Cong, L., Love, M. I., Zhang, F., *et al.* (2014) MAGeCK enables robust identification of essential genes from genome-scale CRISPR/Cas9 knockout screens. *Genome Biol.* **15**, 554
68. Conant, D., Hsiau, T., Rossi, N., Oki, J., Maures, T., Waite, K., *et al.* (2022) Inference of CRISPR edits from Sanger Trace Data, *CRISPR J.* **5**, 123–130
69. Juszkiewicz, S., Chandrasekaran, V., Lin, Z., Kraatz, S., Ramakrishnan, V., and Hegde, R. S. (2018) ZNF598 is a quality control sensor of collided ribosomes. *Mol. Cell* **72**, 469–481.e7
70. Hashimoto, S., Sugiyama, T., Yamazaki, R., Nobuta, R., and Inada, T. (2020) Identification of a novel trigger complex that facilitates ribosome-associated quality control in mammalian cells. *Sci. Rep.* **10**, 3422
71. Segura-Totten, M., Kowalski, A. K., Craigie, R., and Wilson, K. L. (2002) Barrier-to-autointegration factor: major roles in chromatin decondensation and nuclear assembly. *J. Cell Biol.* **158**, 475–485
72. Rohrmoser, M., Holzel, M., Grimm, T., Malamoussi, A., Harasim, T., Orban, M., *et al.* (2007) Interdependence of Pes1, Bop1, and WDR12 controls nucleolar localization and assembly of the PeBoW complex required for maturation of the 60S ribosomal subunit. *Mol. Cell Biol.* **27**, 3682–3694
73. Kellner, M., Rohrmoser, M., Forne, I., Voss, K., Burger, K., Muhl, B., *et al.* (2015) DEAD-box helicase DDX27 regulates 3' end formation of ribosomal 47S RNA and stably associates with the PeBoW-complex. *Exp. Cell Res.* **334**, 146–159
74. Jang, S. H., Kim, A. R., Park, N. H., Park, J. W., and Han, I. S. (2016) DRG2 regulates G2/M progression via the cyclin B1-Cdk1 complex. *Mol. Cells* **39**, 699–704
75. Pakos-Zebrucka, K., Koryga, I., Mnich, K., Ljujic, M., Samali, A., and Gorman, A. M. (2016) The integrated stress response. *EMBO Rep.* **17**, 1374–1395
76. Ceci, M., Gaviraghi, C., Gorrini, C., Sala, L. A., Offenhauser, N., Marchisio, P. C., *et al.* (2003) Release of eIF6 (p27BBP) from the 60S subunit allows 80S ribosome assembly. *Nature* **426**, 579–584
77. Wang, H., Wang, L., Wang, Z., Dang, Y., Shi, Y., Zhao, P., *et al.* (2020) The nucleolar protein NOP2 is required for nucleolar maturation and ribosome biogenesis during preimplantation development in mammals. *FASEB J.* **34**, 2715–2729
78. Box, J. K., Paquet, N., Adams, M. N., Boucher, D., Bolderson, E., O'Byrne, K. J., *et al.* (2016) Nucleophosmin: from structure and function to disease development. *BMC Mol. Biol.* **17**, 19
79. Yamada, S. B., Gendron, T. F., Niccoli, T., Genuth, N. R., Grosely, R., Shi, Y., *et al.* (2019) RPS25 is required for efficient RAN translation of C9orf72 and other neurodegenerative disease-associated nucleotide repeats. *Nat. Neurosci.* **22**, 1383–1388
80. Meola, N., Domanski, M., Karadoulama, E., Chen, Y., Gentil, C., Pultz, D., *et al.* (2016) Identification of a nuclear Exosome decay pathway for processed transcripts. *Mol. Cell* **64**, 520–533